A CAIPI Approach to Decrease Geometry Factor for Simultaneous Multi-Slice Technique in FMRI

Ke Xu[1] and Daniel B. Rowe[2]
[1]Computational Mathematical and Statistical Sciences, Marquette University
1313 W Wisconsin Ave, Milwaukee, WI 53233
[2]Computational Mathematical and Statistical Sciences, Marquette University
1313 W Wisconsin Ave, Milwaukee, WI 53233

Abstract

Functional Magnetic Resonance Imaging (fMRI) enables researchers to study brain functions and advance understanding in human sciences. By detecting the Blood Oxygen Level Dependent (BOLD) contrast signal, spatial and temporal changes in brain metabolism are represented in the frequency domain, known as *k*-space. Traditional MRI methodologies require full *k*-space information, which follows a unique data acquisition sequence to reconstruct the complete image. This process presents a time-consuming obstacle for medical imaging techniques. Therefore, the primary focus of our study is to propose a novel imaging reconstruction method that improves the efficiency of the data acquisition process while maintaining high accuracy in activation detection. In our approach, we introduce a novel two-dimensional acceleration method to expedite the imaging acquisition process. Multiple imaging shift techniques and a new two-dimensional Hadamard aliasing pattern were incorporated to reduce the dependency on aliased voxels and increase the diversity of the acquired information. By applying our approach to both simulated and experimental fMRI data, we successfully reduced the total scan time while achieving higher signal-to-noise ratio (*SNR*) and contrast-to-noise ratio (*CNR*) in regions of interest (ROI). Moreover, compared with traditional imaging reconstruction techniques, our method significantly improves the activation detection rate.

Key Words: fMRI, 2D acceleration, SMS, imaging shift

1. Background

In the functional magnetic resonance imaging (fMRI) study field, the topic of improving the efficiency of data acquisition in the image scanning process has been gaining researchers' interest since 1990. As a noninvasive medical imaging technique, the blood-oxygen-level dependent (BOLD) contrast signal was detected as the proxy reflecting the neuron activation changes through time (Ogawa et al., 1990). In order to acquire the fully sampled spatial frequency space called *k*-space, the gradient echo echo-planer imaging (GRE-EPI) pulse sequence is applied to shorten the scan time and reduce the respiratory artifacts in one excitation (Mansfield, 1977; Rzedzian et al., 1983; Stehling, Turner, and Mansfield, 1991). For each excitation of the GRE-EPI pulse sequence, a zig-zag data-collecting pattern is followed sequentially to form the full *k*-space with each data point representing complex-valued average spatial frequency information within each image. Figure 1 shows the three-dimensional view of the brain image scanning process and the unique data-acquiring sequential pattern in the *k*-space of the GRE-EPI pulse sequence (Sakitis, Brown, and Rowe, 2024). However, to conduct an fMRI experiment, multiple brain images need to be acquired at different

positions, known as volume-image. Thus, it takes a relatively long time to acquire a volume-image fMRI time series in favor of gaining a steady and reliable task-related activation signal.

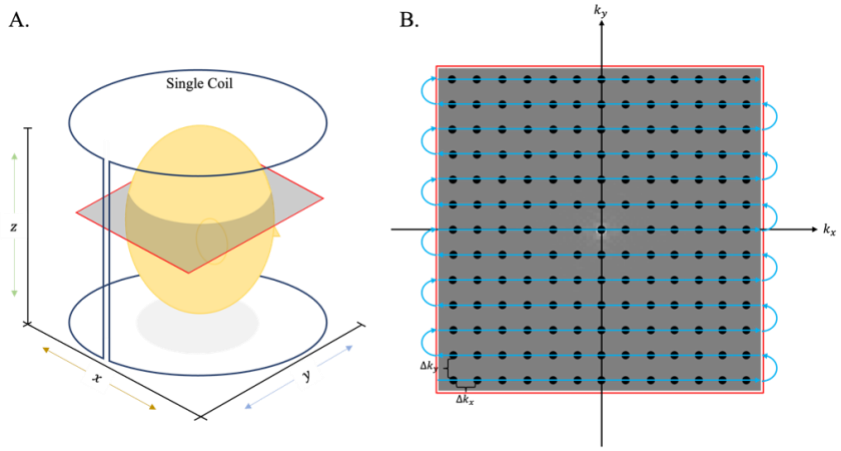

Figure 1. A. The three-dimensional view of brain image acquisition process with one single coil. B. The zig-zag data collecting pattern of GRE-EPI pulse sequence.

In 1986, Hyde introduced a parallel image acquisition technique that incorporated multiple coils, and each coil measured partial sensitivity-weighted spatial frequencies (Hyde et al., 1986). The full brain image can be reconstructed by applying the Sensitivity Encoding (SENSE) approach to combine weighted spatial frequencies from each coil into one single *k*-space array (Pruessmann et al., 1999). In order to reduce the total image scan time, the data acquisition can be accelerated along two dimensions: the in-plane dimension and the through-plane dimension. The in-plane acceleration (IPA) method aims at expediting the single slice readout process by skipping partial lines in the *k*-space. As an alternative to SENSE, the unacquired spatial frequency point can be estimated by the application of the generalized autocalibrating partially parallel acquisition (GRAPPA) approach (Griswold et al., 2002). Prior information on missing data in the *k*-space can be acquired from the calibration images. Figure 2 shows the three-dimensional view of the brain image acquisition process with four receiver coils and the subsampled spatial frequence domain for IPA approach with acceleration factor $IPA = 2$ (Sakitis, Brown, and Rowe, 2024). In Figure 2B, every other line in the *k*-space, black dots, is acquired, and the white dots line is skipped. However, the total scan time does not decrease with the factor of the IPA due to fixed time blocks in the data-acquiring process like proper time to T_2^* contrast and imaging encoding time in one excitation. The through-plane acceleration (TPA) approach, on the other hand, focuses on expediting the image acquisition process by acquiring multiple images simultaneously in one excitation. The spatial information for multiple images is not acquired separately, instead, is aliased into one single *k*-space for each excitation. Techniques like the simultaneous multi-slice (SMS) approach can be incorporated with the TPA approach by applying a multiband (MB) radiofrequency (RF) within a reduced repetition time (TR) (Souza et al., 1988; Rowe et al., 2013; Barth et al., 2016; Rowe et al., 2016). Compared with the IPA approach, the TPA approach can improve the efficiency of the data-acquiring process more significantly, with the total scan time being reduced with a fraction of the TPA acceleration factor.

To further reduce the total image scan time and achieve the ultimate goal of our study, we introduce a novel SMS image reconstruction technique called a controlled aliasing in parallel imaging with view angle tilting approach and in-plane acceleration method for multi-coil separation of parallel encoded complex-valued slices (mSPECS-IPA-CAIPIVAT) will be presented and discussed. This study is developed upon the mSPECS-IPA approach with TPA and IPA acceleration techniques combined into a two-dimensional acceleration technique (Kociuba, 2016). Through the two-dimensional acceleration technique, a higher acceleration factor can be achieved. In the novel image

reconstruction method, we incorporate an image shift technique into the model to decrease the similarity of the coil sensitivity information for the aliased voxels. More detail will be discussed in the Section 2.

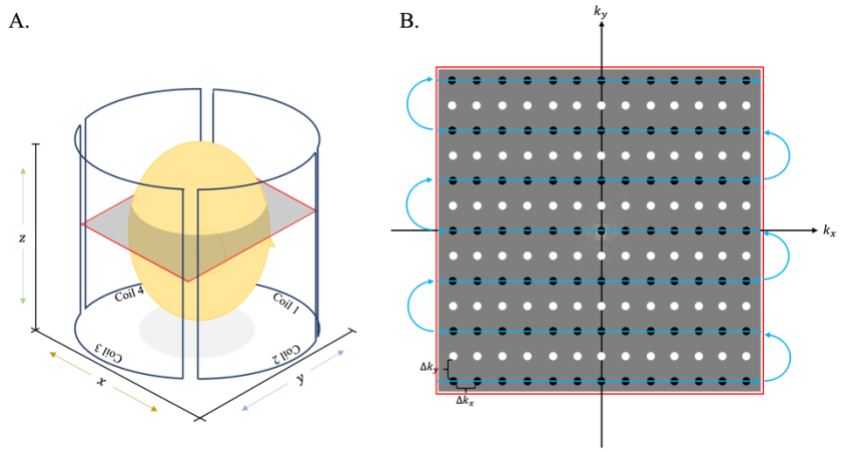

Figure 2. A. The three-dimensional view of brain image acquisition process with four coils. B. The subsampled spatial frequency domain incorporated with IPA approach and the acceleration factor equal to 2.

2. Theory

2.1 Data Acquiring Process

2.1.1 Image Shift Techniques

As discussed in Section 1, the SMS technique can acquire images of multiple brain slices concurrently and the total volume scan time can be reduced dependent on the selected TPA factor. Figure 3 shows the 3D and 2D view of the image acquiring process with four slices and four coils. Different from the single slice acquisition process, the multiple slice acquisition process leads to the short physical distance between aliased images. When applying the SENSE approach to reconstruct brain images and capture the activity signal, an ill conditioned matrix problem occurs caused by the high similarity of the coil sensitivity information between the short-distanced aliased voxels. Thus, a strong inter-slice signal and anatomical structure from other slices will appear on the reconstructed images. To determine the performance of the image reconstruction method with high acceleration factors, the noise amplification factor or geometry factor, *g*-factor, is defined by (Setsompop et al., 2012; Welvaert and Rosseel, 2013):

$$g_{SMS} = \frac{SNR_{full}}{SNR_{accelerate}\sqrt{R}}. \quad (1)$$

In Eq. 1, SNR_{full} is the signal-to-noise (*SNR*) ratio for the reconstructed images from techniques without acceleration factors, $SNR_{accelerate}$ is the *SNR* value for the reconstructed images with acceleration factors, and *R* is the IPA factor. According to Eq. 1, high similarity of coil sensitivity information induces the high g_{SMS} value, which leads to a reduction of the $SNR_{accelerate}$ ratios for the reconstructed images. Thus, to increase the $SNR_{accelerate}$ value and improve the performance of the novel acceleration technique, we introduce the image shift methods to manually increase the physical distance between aliased voxels.

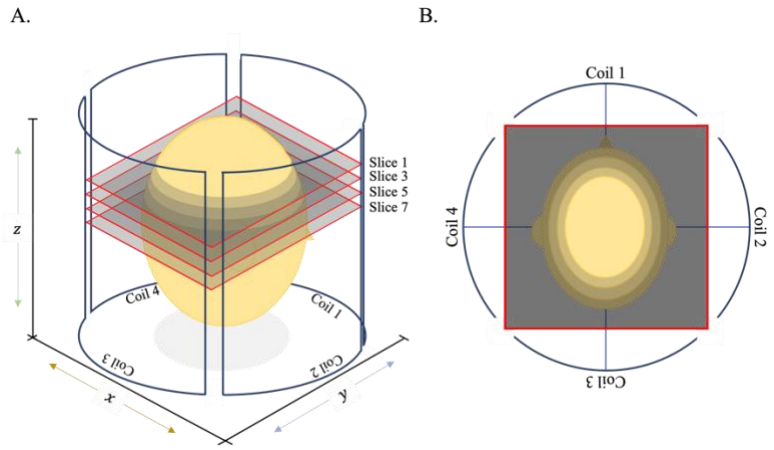

Figure 3. A. The 3D view of SMS technique with four slices and four coils acquisition process at one excitation. B. The 2D view for the same process with four slices and four coils.

For each excitation, the brain image can be shifted along three directions: the phase-encoding (PE) direction (vertically in this study, notation "↑" and "↓" means image shift up and down), the readout (RO) direction (horizontally in this study, notation "←" and "→" means image shift left and right), and PE and RO direction (vertically and horizontally at the same time in this study, notation "↗", "↖", "↘", "↙" indicates the direction images shift to). To decrease the influence of the geometric properties of the coil sensitivity maps, techniques like "controlled aliasing in parallel imaging results in higher acceleration" (CAIPIRINHA) and "blipped-CAIPIRINHA" (Blipped-CAIPI) provide other possible ways to minimize the influence of the *g*-factor and maximize the physical distance of the aliased voxels (Breuer et al., 2005; Setsompop et al., 2012). The CAIPIRINHA approach can shift the images along the PE direction by modulating the phase for each line in the *k*-space and imparting each line with a specific angle. Applying a unique phase modulation amount to each slice in the aliased image-acquiring process increases the physical distance between the aliased voxels. Therefore, the independence of coil sensitivity for each slice will increase, and the influence of the *g*-factor for each excitation will be minimized. Moreover, to shift the brain image along the RO direction, a technique like the view angle tilting (VAT) approach applies compensation gradients to the slice selection direction to correct the chemical-shift artifacts in the image scanning process (Cho, Kim, D. J., and Kim, Y. K., 1988; Min-Oh Kim et al., 2012). The distance shifted along the RO direction is relate to the view angle θ in the data acquisition process. The CAIPIRINHA and the VAT technique can be combined, and thus the study "multislice CAPIPRINHA using view angle tilting technique" (CAIPIVAT) proposed (Jungmann et al., 2015; Min-Oh Kim et al., 2016). Through this technique, the FOV can be shifted along the PE and RO direction by applying different amounts of phase modulation to each line in the *k*-space and the compensation gradients on the slice selection direction together for each excitation. Figure 4 shows the *k*-space for CAIPIRINHA and CAIPIVAT techniques along the reconstructed brain images after the inverse Fourier transform.

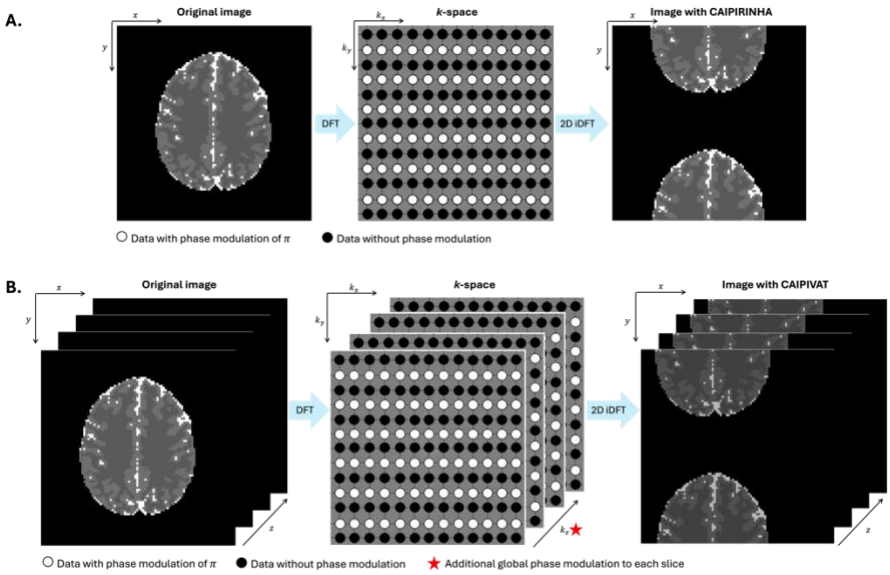

Figure 4. A. An illustration of the CAIPIRINHA process. B. An illustration of the CAIPIVAT process.

In this study, the principal idea of the CAIPIRINHA technique will be applied first. For each slice within each excitation, we imply $\Delta y = (l-1)FOV/N_s$ in-plane image shift, where $l = 1, \dots, N_s$ and N_s is the total number of aliased slices. On the TR dimension, we also imply the CAIPIRINHA technique for each excitation by $\Delta y = (m-1)FOV/N_s$ in-plane image shift, where $m = 1, \dots, N_s$. Thus, with the in- and through-excitation image shift, at $TR = N_s + 1$ excitation time point, the aliased artifacts should be the same as the $TR = 1$ excitation time point. Figure 5A shows an example of an in- and through-excitation image shifts process with $N_s = 4$ incorporating with the CAIPIRINHA technique. When $TR = 5$, the image shift pattern for each slice should be the same as the time point $TR = 1$. Furthermore, the principal idea of the CAIPIVAT technique will also be applied. Similar to the CAIPIRINHA technique, $\Delta y = (l-1)FOV/N_s$ for the in-plane image shift and by $\Delta y = (m-1)FOV/N_s$ for the through-plane image shift will be applied to each excitation along the PE direction. For each slice within each excitation, a unique image shift will appear horizontally on the RO direction with the support of the CAIPIVAT technique. The shift distance for each slice along the RO direction can be calculated and depends on the distance between the desired aliased slices, the compensation gradient, and the RO gradient. A modest slice-wise shift will be applied for each excitation to ensure the brain image is not outside the FOV. Figure 5B displays an example of in- and through-excitation image shift process of $N_s = 4$ incorporating with the CAIPIVAT technique. Besides the same amount of the FOV shift in- and through-excitation on the PE direction as the CAIPIRINHA technique, slice 1 and slice 3 will have a FOV shift to the left as well as slice 2 and slice 4 will have a FOV shift to the right on the RO direction according to the CAIPIVAT technique. Thus, compared with the CAIPIRINHA technique approach, the overlapping area between two desired aliased images will decrease and the independency of the sensitivity for each coil will increase. Moreover, based on the sequential properties, the image shift pattern for each slice should be the same as the time point $TR = 1$ when $TR = 5$.

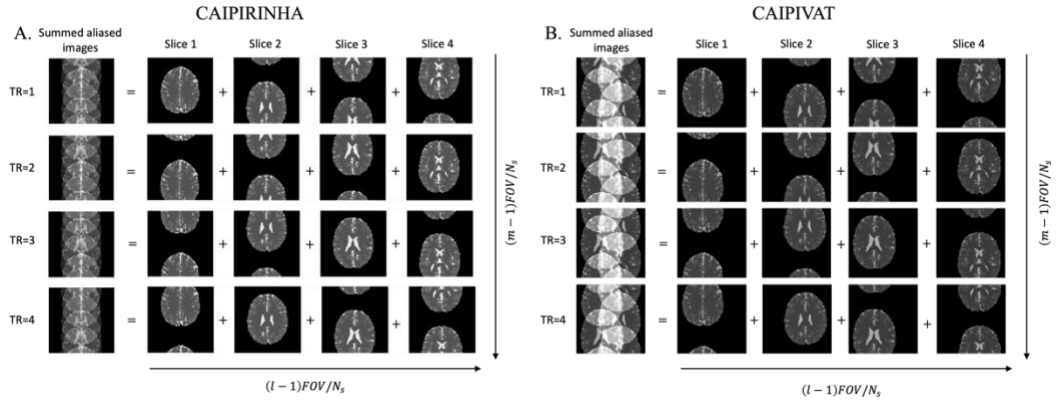

Figure 5. A. An example of in- and through-excitation image shift process with $N_s = 4$ by applying the CAIPIRINHA technique. B. An example of in- and through-excitation image shift process with $N_s = 4$ by applying the CAIPIVAT technique.

2.1.2 Two-Dimensional Hadamard Phase Encoding

The Hadamard encoding technique is a well-developed volume excitation method (Souza et al., 1988). The conventional magnetic resonance (MR) imaging techniques have been limited by the size of the matrix for the acquired aliased images. The Hadamard phase encoding method allows the increment of the size of the acquired aliased image matrix by aliasing in both frequency and phase encoding dimensions. With the support of this simultaneous binary-encoded technique, the TR will decrease, and the *SNR* ratio will improve. The Hadamard matrix is given by:

$$H_{2^n} = \begin{bmatrix} H_{2^{n-1}} & H_{2^{n-1}} \\ H_{2^{n-1}} & -H_{2^{n-1}} \end{bmatrix} = H_2 \otimes H_{2^{n-1}}, with\ H_1 = [1], H_2 = \begin{bmatrix} 1 & 1 \\ 1 & -1 \end{bmatrix}, \quad (2)$$

where $\otimes$ denotes the Kronecker product. It is an orthogonal and full rank matrix with elements of either +1 or -1. In this study, since the TPA approach and the IPA approach are combined to further decrease the total image scan time, and the image shift techniques are incorporated to decrease the influences of the geometry properties, we introduce a novel two-dimensional Hadamard phase encoding technique to our approach. The novel two-dimensional Hadamard phase encoding technique is developed and based upon the Hadamard phase encoding technique with elements of either +1 or -1. However, different from the Hadamard phase encoding technique, in order to guarantee the orthogonality property for each aliased image, different Hadamard coefficients will be assigned to different segments for different slices. Figure 6 shows the two-dimensional Hadamard phase encoding aliasing coefficient for $N_s = 2$ and $N_s = 4$ situations. First, for each excitation or each TR, the through-plane Hadamard coefficient will be assigned to different slices. Second, for each segment of each slice, the in-plane Hadamard coefficient will be assigned to a different excitation. To maintain the orthogonality property for each segment of each slice, the in-plane Hadamard coefficient starts from the second column of the Hadamard coefficient for the first excitation. At the last TR of the cycle, the in-plane Hadamard coefficient is the first column of the Hadamard matrix. Finally, the two-dimensional Hadamard coefficient will be the product of the through-plane and in-plane Hadamard coefficient for each segment of each slice and each excitation. The size of the in-plane and through-plane Hadamard coefficient matrix is equal to the number of aliased slices for each excitation N_s.

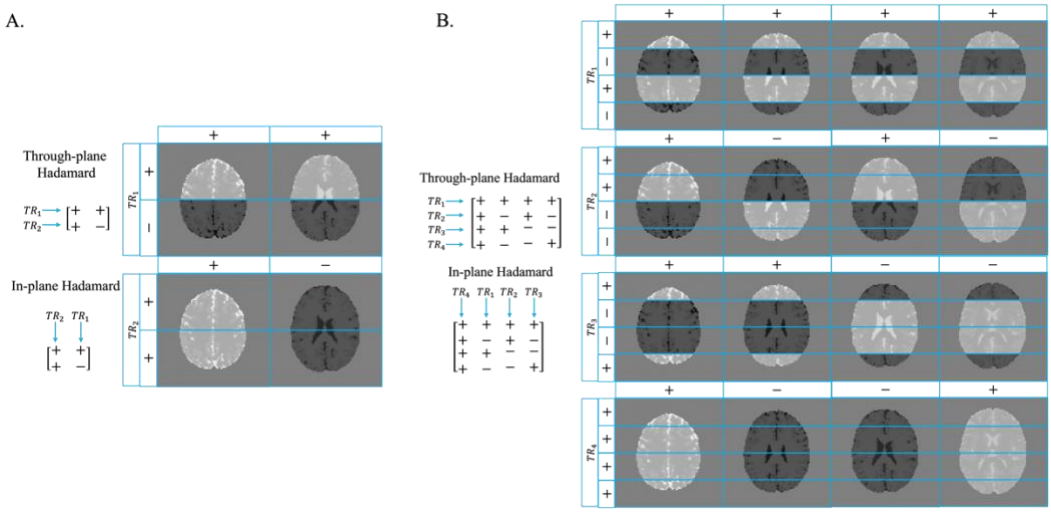

Figure 6. A. The two-dimensional Hadamard phase encoding coefficient for $N_s = 2$. B. The two-dimensional Hadamard phase encoding coefficient for $N_s = 4$.

2.1.3 A Single Aliased Voxel

Given a single aliased voxel, $a_{j,\gamma,\delta}$, at the location (x, y) of aliased images, with δth Hadamard aliasing pattern and γth matrix rotation operation, measured at coil j, is defined as the summation equation:

$$a_{j,\gamma,\delta} = \sum_{m=1}^{R} \sum_{z=1}^{N_S} H_{\delta,z,m} R_{\gamma,z,m} S_{j,z,m} \beta_{z,m} + \varepsilon_j . \tag{3}$$

In Eq. 3, $a_{j,\gamma,\delta}$ is a 2×1 complex-valued vector with the real and imaginary components of the acquired aliased voxel value measured at coil j, with rotating operation γ and Hadamard phase-encoding aliasing pattern δ. The Hadamard phase-encoding aliasing pattern, $H_{\delta,z,m}$, is the same as the definition in Section 2.1.2, where parameter δ corresponds to the order of Hadamard coefficients pattern, parameter z corresponds to the number of slices, and parameter m corresponds to the IPA factor. The coefficients of $H_{\delta,z,m}$ will be either +1 or -1. The matrix rotation operator, $R_{\gamma,z,m}$, is closely related to the definition of Section 2.1.1. Subscript γ denotes the order of the matrix rotation operation for each TR, and parameter z corresponds to the number of slices. The coil sensitivity matrix, $S_{j,z,m}$, is a 2×2 skew symmetric matrix with the real and imaginary components at coil j for slice z, $S_{(j,z,m)} = [S_R, -S_I; S_I, S_R]_{j,z,m}$. The true voxel value, $\beta_{z,m}$, is a 2×1 vector with the real and imaginary parts of the aliased voxel in slice z. The measurement noise, ε_j, is a 2×1 vector with real and imaginary parts. The mean of measurement noise is $E(\varepsilon_j) = 0$, and the covariance of error is $cov(\varepsilon_j) = \sigma^2 I_2$, where I_2 is a 2×2 identity matrix. There is no correlation between the real and imaginary parts of measurement error.

Considering the measured aliased voxel in Eq. 3 across the N_c coils for N_s aliased slices with N_α time-points in the fMRI time series, Eq. 3 can be expressed as:

$$a = X_A \beta + \varepsilon. \tag{4}$$

N_α denotes the number of sequential time-points of the Hadamard encoded pattern, and it is an integer between 1 and N_s. Therefore, the net acceleration of the fMRI time series acquisition is defined as $A = N_s R/N_\alpha$. In Eq. 4, the dimension of a is $2N_c N_\alpha \times 1$ including the real and imaginary components. The measurement error, ε, has the same dimension as a with the mean $E(\varepsilon) = 0$ and covariance $cov(\varepsilon) = \sigma^2 I_{2N_c N_\alpha}$. The dimension of the aliasing matrix, X_A, is $2N_c N_\alpha \times 2N_s N_r$, where N_r is an indicator of the number of matrix rotation operations. In this study, we generally assign $N_r = N_s$ to improve the computational efficiency. The true voxel value, β, has the dimension of $2N_s N_r \times 1$, including the real and imaginary value for each voxel. For the δth Hadamard aliasing pattern and γth matrix rotating operation, the aliasing matrix $(X_A)_{\gamma,\delta}$ across N_c coils is defined as:

$$(X_A)_{\gamma,\delta} = \left[H_{\delta,1} R_{\gamma,1} \begin{pmatrix} S_{1,1} \\ \vdots \\ S_{N_c,1} \end{pmatrix}, \dots, H_{\delta,N_s} R_{\gamma,N_s} \begin{pmatrix} S_{1,N_s} \\ \vdots \\ S_{N_c,N_s} \end{pmatrix} \right]. \quad (5)$$

$R_{\gamma,z}$ is the image shift indicator which operates on coil sensitivity maps for each slice, and it is not the matrix multiplication. Across the N_α excitations, the aliasing matrix X_A can be written as:

$$X_A = \begin{bmatrix} (X_A)_1 \\ \vdots \\ (X_A)_{N_\alpha} \end{bmatrix}. \quad (6)$$

To separate the aliased images and estimate the voxel value for each slice, the least square estimation method is used. The estimated separate voxel value, $\hat{\beta}$, can be calculated by:

$$\hat{\beta} = (X_A' X_A)^{-1} X_A' a. \quad (7)$$

In general, the determinant of X_A is close to zero, $\det(X_A) \approx 0$, which leads to failure in calculating the inverse of $X_A' X_A$. Thus, a bootstrap sampling method incorporated with the artificial aliasing of reference calibration images technique is combined with the mSPECS-IPA-CAIPIVAT method. This combined technique can eliminate the inter-slice signal leakage artifacts by introducing a regularizer in the least square estimation function and making the aliasing matrix to be full rank for the inverse. More details will be shown in the following section. Figure 7 shows acquired voxel aliasing situation for each two-dimensional acceleration image reconstruction technique. The top row is the acquired image voxel aliasing situation for mSPECS-IPA technique that no image shift technique is incorporated with $N_s = 4$. The middle row shows the acquired image voxel aliasing situation for mSPECS-IPA-CAIPIRINHA technique that images can be shifted vertically with $N_s = 4$. The bottom row shows the acquired image voxel aliasing situation of mSPECS-IPA-CAIPIVAT technique that images can be shifted horizontally and vertically with $N_s = 4$. As Figure 7 shows, the image overlapping area is decreasing from mSPECS-IPA to mSPECS-IPA-CAIPIVAT technique, which intuitively make the image reconstruction process easier compared with non-image shift technique.

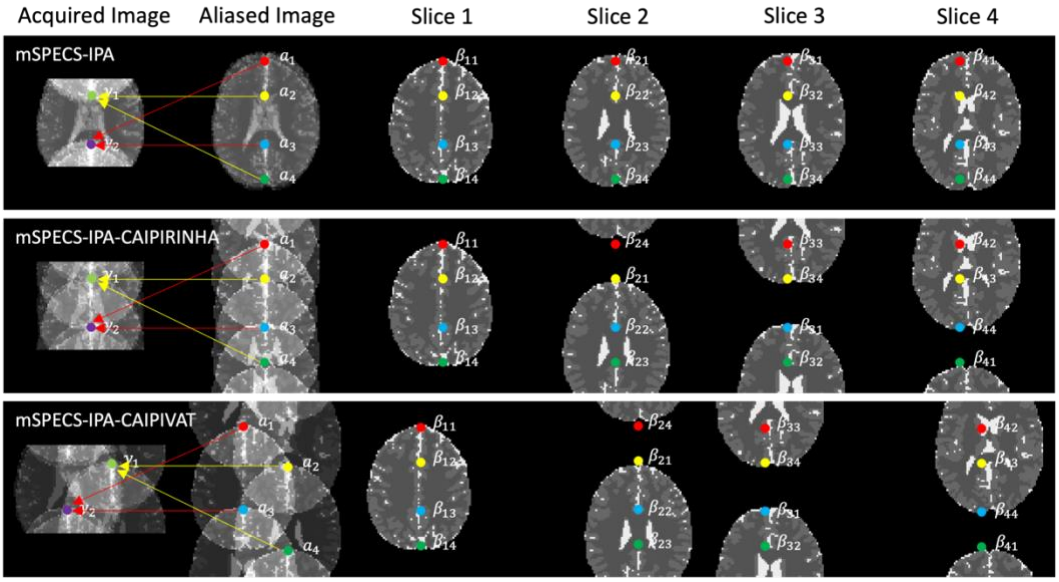

Figure 7. The acquired image voxel aliasing situation for mSPECS-IPA with $N_s = 4$ (top). The acquired image voxel aliasing situation for mSPECS-IPA-CAIPIRINHA with $N_s = 4$ (middle). The acquired image voxel aliasing situation for mSPECS-IPA-CAIPIVAT with $N_s = 4$ (bottom).

2.2 The Bootstrap Sampling and Artificial Aliasing of Calibration Images

In the previous simultaneous multi-slice (SMS) study, bootstrap sampling and artificial aliasing of calibration reference image techniques have been proven as powerful tools to support the separation and reconstruction process of aliased images. By increasing the size of the aliasing matrix and adding a regularizer into the least square estimation function, the correlation induced by the separation process will decrease and the slice-to-slice signal leakage will be eliminated. In the fMRI time series, for each excitation, N_s bootstrap sampled coil slice images will be randomly chosen from fully sampled calibration reference images. The mean calibration images will be calculated for each slice and will be artificially aliased which is then repeated for each TR.

Given a single TR, the calibration images will have the same shift pattern as acquired images, thus, the total number of different combinations for different voxels should be N_s, which is equal to the rank of the chosen Hadamard matrix. After removing the combination of the acquired aliasing pattern from the full voxel combination pattern, $N_s - 1$ different combinations remain. Therefore, for a single excitation, a voxel across N_s slices, measured through N_c coils, ν, can be represented as a vector with the dimension of $2N_sN_c(N_s - 1) \times 1$ with the real component stacked on the top of the imaginary component, corresponding to the remain combinations without the acquired aliasing combination. The mean bootstrap sampled voxel, $\bar{\nu}$, is the same dimension as ν for each time point. The artificial aliasing calibration images, ν, across N_s slices measured through N_c coils at N_α sequential time point can be expressed as:

$$\nu = C\bar{\nu} = C_A\mu + C\eta. \tag{8}$$

The dimension of the measurement error vector, η, is the same size as the vector ν. The mean of the measurement error for the calibration images is $E(\eta) = 0$, and the covariance is $cov(C\eta) = \sigma^2 I_{2N_s N_c(N_s-1)}$, where $I_{2N_s N_c(N_s-1)}$ is the identity matrix. There is no correlation between the real and imaginary components of the calibration images. The true voxel value vector, μ, is constructed with the real and imaginary components of the calibration voxel with the dimension $2N_s \times 1$. The artificial aliasing matrix, C_A, is following the same aliasing rules as acquired images do, rotating by the matrix rotation operation and multiplying the Hadamard encoding aliasing coefficients. Due to the combination of acquired aliasing voxel removed from the full combinations, the dimension of the artificial aliasing matrix is $2N_s N_c(N_s - 1) \times 2N_s$. Same as the assumption in the acquired aliasing images, we assign $N_r = N_s$ to improve the computational efficiency. For example, considering a situation with $N_s = 4$ and $N_r = 4$, for each time point, $N_s - 1 = 3$ combinations should be applied for the calibration images. Thus, for a given excitation, the δth Hadamard aliasing pattern and γth matrix rotating operation, the aliasing matrix $(C_A)_{\gamma,\delta}$ across N_c coils can be written as:

$$(C_A)_{\gamma,\delta} = \left[\overline{H_{\delta,1}R_{\gamma,1}}\begin{pmatrix} S_{1,1} \\ \vdots \\ S_{N_c,1} \end{pmatrix}, \dots, \overline{H_{\delta,N_s}R_{\gamma,N_s}}\begin{pmatrix} S_{1,N_s} \\ \vdots \\ S_{N_c,N_s} \end{pmatrix}\right]. \tag{9}$$

The notation $\overline{HR}$ denotes the remaining combination for the Hadamard encoding aliasing pattern with the matrix rotation pattern after removing the combination of the acquired aliasing pattern. Incorporating N_α sequential time points, the artificial aliasing matrix, C_A, can be written as:

$$C_A = \begin{bmatrix} (C_A)_1 \\ \vdots \\ (C_A)_{N_\alpha} \end{bmatrix}. \tag{10}$$

2.3 The Statistical Separation Process

To separate the aliased voxel, according to the mSPECS-IPA-CAIPIVAT approach, we combine Eq. 4 and Eq. 8 together, which will generate:

$$y = \begin{bmatrix} a \\ \nu \end{bmatrix} = \begin{bmatrix} X_A\beta \\ C_A\mu \end{bmatrix} + \begin{bmatrix} \varepsilon \\ C\eta \end{bmatrix}. \tag{11}$$

The dimensions for each parameter in the equation are discussed in detail in the previous sections. The least squares estimation function is incorporated with the mSPECS-IPA-CAIPIVAT method, which will lead us to:

$$\hat{\beta} = (X_A'X_A + C_A'C_A)^{-1}(X_A'a + C_A'\nu). \tag{12}$$

$C_A'C_A$ works as the regularizer for the matrix inverse to improve the condition of the equation. The expectation value of the estimation images is:

$$E(\hat{\beta}) = (X_A'X_A + C_A'C_A)^{-1}(X_A'\beta + C_A'\mu). \tag{13}$$

Based on the previous section, the covariance for the acquired aliasing measurement error is $cov(\varepsilon) = \sigma^2 I_{2N_c N_\alpha}$, and the covariance for the artificial aliasing measurement error is $cov(C\eta) =$

$\sigma^2 I_{2N_S N_c (N_S N_r - 1)}$, the covariance for vector, y, consisting of acquired aliasing voxel value and the artificial aliasing voxel value is:

$$cov(y) = \begin{bmatrix} \sigma^2 I_{2N_c N_\alpha} & 0 \\ 0 & \tau^2 I_{2N_S N_c (N_S N_r - 1)} \end{bmatrix}. \quad (14)$$

Without the support of the bootstrapping technique, there will be no variation in the artificial aliasing calibration images, i.e. the same calibration reference images will be artificially aliased for each TR, which will lead to $\tau^2 = 0$. The correlation induced by the separation process will increase and exhibit slice-to-slice signal leakage artifacts. With the help of the bootstrap sampling approach, $\tau^2 = \sigma^2$, such that the covariance of $\hat{\beta}$ is:

$$cov(\hat{\beta}) = \sigma^2 (X_A' X_A + C_A' C_A)^{-1}. \quad (15)$$

Therefore, the correlation induced by the unaliasing process is minimized, and the inter-slice signal leakage artifacts are eliminated.

3. Simulation Study

3.1 Simulated FMRI Data

To investigate the performance of our proposed novel SMS technique, the mSPECS-IPA-CAIPIRINHA, and the mSPECS-IPA-CAIPIVAT model were applied to simulated fMRI data, and the results were compared with the mSPECS-IPA. The simulated fMRI data has $TR = 510$ time points and mimics the real-world right hand finger tapping fMRI experiment. The first 20 time points will be omitted, thus leaving the simulated fMRI data with 490 time points. To replicate the full process of the real right-handed finger-tapping experiment, two time series were generated from the true noiseless axial view data: the calibration simulated data, and the task simulated data. The calibration simulated data includes $N_S = 8$ axial brain images without any simulated task activation blocks for each image. The task simulated data, in contrast, includes $N_S = 8$ axial brain images with simulated task activation blocks on the left motor cortex for the first 4 slices. No simulated activation blocks were added to the other 4 slices. The simulated activation blocks were added according to the in vivo experiment design, with the first 20 TRs off, following 15 TRs on and 15 TRs off for 16 epochs, and the last 10 TRs off. To achieve the $CNR = 0.5$, the mean magnitude of 0.04 was added to the simulated activation blocks for the first 4 slices. The mean magnitude of 4, to achieve $SNR = 50$, and different phase angles from 5° to 40° with 5° intervals were added to each image. In order to further increase the distinction of the spatial information for different tissue type, angle 7.5° was added to white matter (WM), 15° was added to gray matter (GM), and 22.5° was added to the cerebral spinal fluid (CSF). Gaussian distribution noise $N(0,0.0064)$ was added for each image of the calibration simulated data and the task simulated data separately. Figure 8A shows the true noiseless simulated magnitude and true phase information for $N_S = 8$ axial brain images.

A total of $N_C = 8$ channel coil sensitivity profiles were simulated to weight each axial brain image. A mean magnitude of 0.95 and the different phase angles from 0° to 17.5° with 2.5° intervals were applied to each coil sensitivity. Figure 8B shows the simulated magnitude and phase information of the $N_C = 8$ channel coil sensitivity profiles for the third axial brain image (slice 3). In the interest of investigating our new proposed SMS techniques under different TPA factors, we applied our model to three acceleration scenarios: TPA=2 (packet 1: slice 1 and 5, packet 2: slice 2 and 6, packet 3: slice 3 and 7, and packet 4: slice 4 and 8), TPA=4 (packet 1: slice 1, 3, 5 and 7, packet 2: slice 2, 4, 6 and 8), and TPA=8 (all slices into one packet). The number of packets multiplied by the acceleration factor equals to the total number of images. All experiments were performed on MATLAB program software.

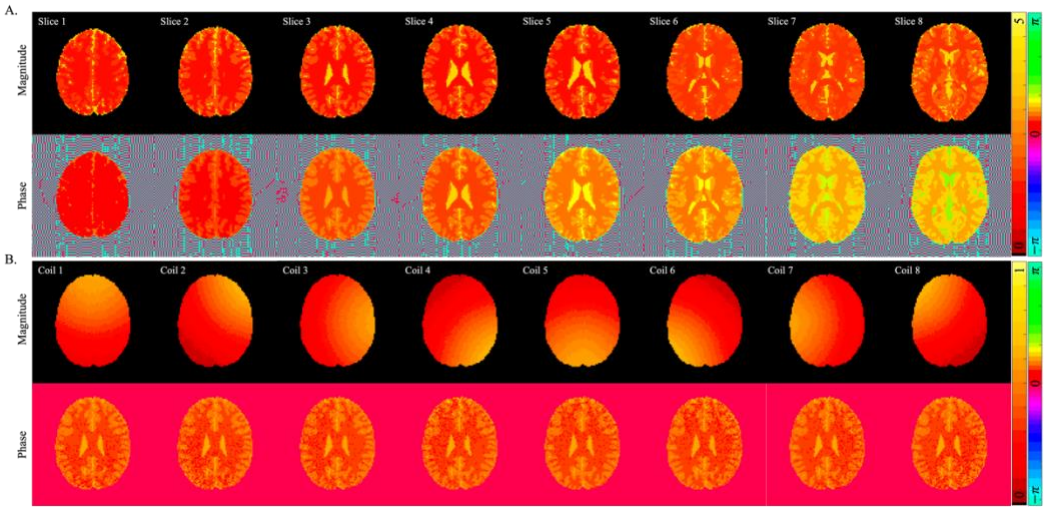

Figure 8. A. The true noiseless simulated magnitude and true phase information for axial brain images. B. The simulated magnitude and phase information of $N_C = 8$ channels coil for slice 3.

3.2 Simulated Reconstruction Results

Following the methodology of the mSPECS-IPA-CAIPIVAT in Section 2, we conducted the simulated fMRI experiment with different combinations of in-plane and through-plane acceleration factors: IPA=2 and TPA=2, IPA=2 and TPA=4, and IPA=2 and TPA=8. Under these three circumstances, the net acceleration factor will be achieved at 4, 8, and 16. Figure 9 shows the temporal mean magnitude and the temporal mean phase of slice 3 of the reconstructed images from the mSPECS-IPA, mSPECS-IPA-CAIPIRINHA, and the mSPECS-IPA-CAIPIVAT approach and compared with the true noiseless magnitude and the true noiseless phase. Compared with the true value, these three methods provide clear reconstructed brain images with detailed anatomical information. However, comparing the background noise of the phase, the noise level increasing from the mSPECS-IPA to mSPECS-IPA-CAIPIVAT approach, and the mSPECS-IPA-CAIPIVAT approach has the highest background phase noise among these three methods.

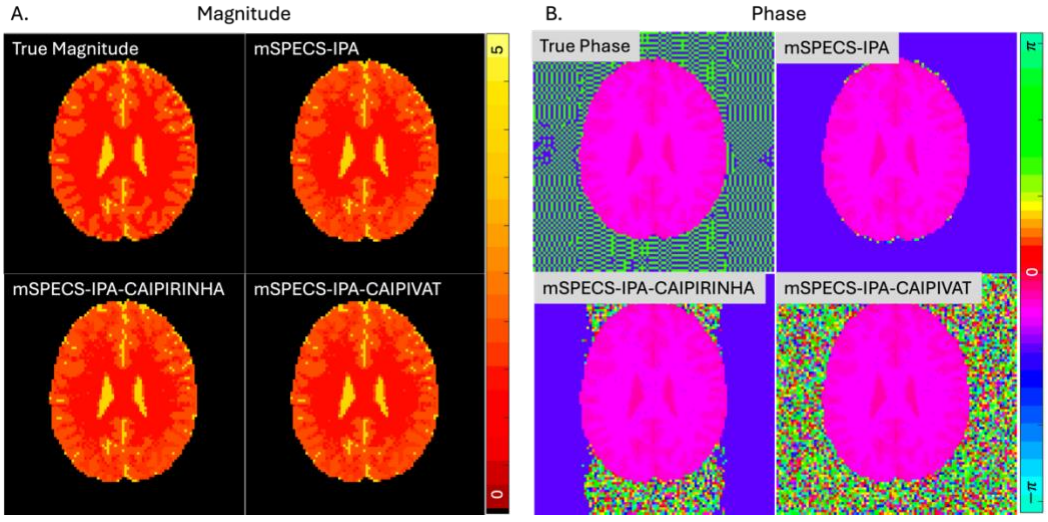

Figure 9. The true noiseless magnitude and true noiseless phase comparing with the temporal mean magnitude and phase from mSPECS-IPA, mSPECS-IPA-CAIPIRINHA, and mSPECS-IPA-CAIPIVAT for slice 3.

To evaluate the performance of the novel two-dimensional acceleration image reconstruction approach, the *SNR* value and the task activation detection rate were compared with these three models. The temporal signal-to-noise ratio is defined as $SNR = \bar{S}/\sigma_N$, where $\bar{S}$ is the mean magnitude value in the time series, and σ_N is the standard deviation of the noise. The signal-to-noise ratio also can be expressed as $SNR = \beta_0/\sigma_N$, where β_0 is the baseline signal, and σ_N is the standard deviation of the magnitude of the noise. Activation detection was performed using a complex-valued model to compute fMRI activation (Rowe and Logan, 2004). Figure 10 shows the *SNR* and the activation detection rate for ROI of slice 3 from the mSPECS-IPA, mSPECS-IPA-CAIPIRINHA and the mSPECS-IPA-CAIPIVAT method. As Figure 10A shows, the mSPECS-IPA-CAIPIRINHA has the lowest average *SNR* of ROI, whereas the mSPECS-IPA and the mSPECS-IPA-CAIPIVAT method has a close *SNR* value of ROI. However, comparing the activation detection rate of ROI, which is the z-score, the mSPECS-IPA-CAIPIVAT method provides the highest average activation detection value for ROI and the mSPECS-IPA-CAIPIRINHA has the lowest score. From the activation detection value of three methods, the mSPECS-IPA-CAIPIVAT has higher significance to capture the brain task-related signal.

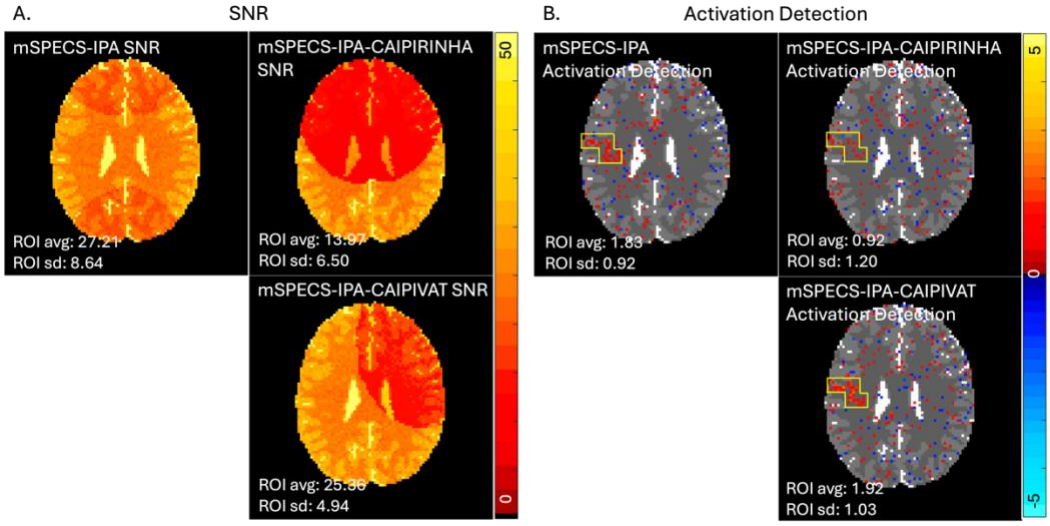

Figure 10. The average *SNR* and the average activation detection rate of ROI for slice 3 from mSPECS-IPA, mSPECS-IPA-CAIPIRINHA and mSPECS-IPA-CAIPIVAT model.

4. Experimental FMRI Study

4.1 Experimental FMRI Data

A 3.0 T General Electric Signa LX MRI scanner was used to perform a right-handed finger-tapping fMRI experiment on a single object. The experiment was designed with an initial 20s of rest, following 15s off and 15s on for 16 epochs, and a final 10s of rest. This results in a time series with 510 time repetitions was acquired for each repetition lasting 1s. The first 20s were disregarded leading to a time series with 490 time repetitions. An additional non-task time series was also acquired from the same object to serve as calibration time series. A flip angle of 90° with an acquisition bandwidth of 125kHz was applied in this experiment. The thickness of the axial brain images slice was 2.5 mm with 9 slices for each time repetition. Due to the nature of the Hadamard phase-encoding method, 8 slices were used for the new proposed reconstruction models and compared with the existing models. The most inferior axial brain slice was disgarded. An 8-channel receiver coil was applied with dimension 96×96 for a 24 cm full FOV. The phase encoding

direction is posterior to anterior. In order to acquire the "true" reconstruction brain images and activation signals, the SENSE model was applied to each time repetition without any through-plane acceleration method, and the reconstructed images were treated as reference reconstruction images. Reconstruction results from mSPECS-IPA, mSPECS-IPA-CAIPIRINHA and mSPECS-IPA-CAIPIVAT model were compared to the reference reconstruction images.

4.2 Experimental Reconstruction Results

In order to investigate the performance of the novel slice-wise image shift SMS models on a real-world experiment, we applied mSPECS-IPA-CAIPIRINHA and mSPECS-IPA-CAIPIVAT model to the right-handed finger-tapping fMRI experiment time series. Reconstructed axial brain images were obtained from these two image-shifting models and compared with the reconstruction results from the mSPECS-IPA model; reference images were also included in the comparison. We also investigated the model performance of the novel slice-wise image shift models with different in-plane and through-plane acceleration factors: IPA=2 and TPA=2, IPA=2 and TPA=4, and IPA=2 and TPA=8, and compared the reconstruction results with the mSPECS-IPA model. Figure 11 shows the temporal mean magnitude and temporal mean phase of slice 3 from mSPECS-IPA, mSPECS-IPA-CAIPIRINHA, and mSPECS-IPA-CAIPIVAT model and compared with the reference mean magnitude and mean phase reconstructed from the SENSE technique. As Figure 11 shows, the mSPECS-IPA, mSPECS-IPA-CAIPIRINHA, and mSPECS-IPA-CAIPIVAT methods provide clear and high-resolution reconstructed brain image with detailed anatomical structures inside of brian, and the mean magnitude and mean phase from these three models are close to the reference magnitude and phase. However, similar to the simulation results, the mSPECS-IPA-CAIPIVAT model has the highest background phase noise, and the mSPECS-IPA provides the lowest phase noise.

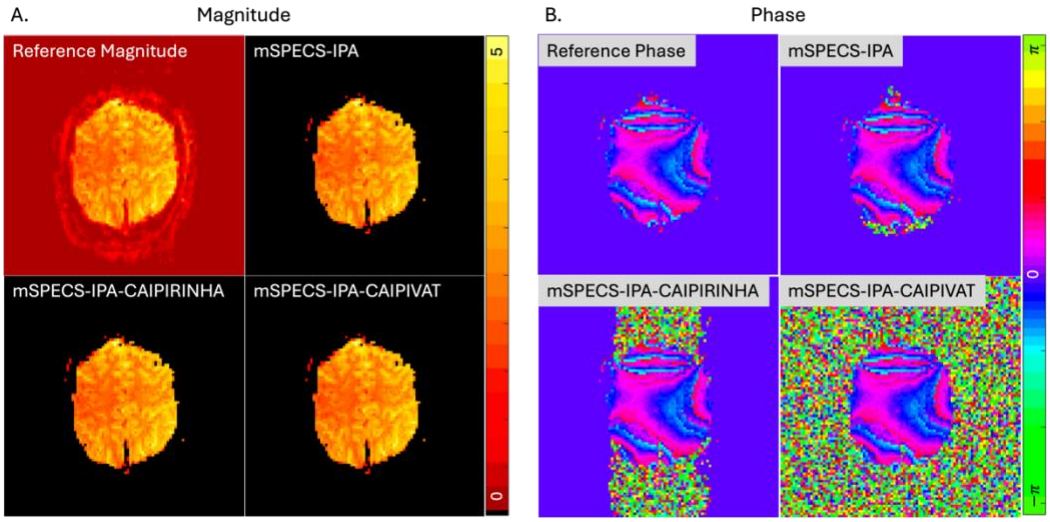

Figure 11. The reference magnitude and reference phase comparing with the temporal mean magnitude and phase from mSPECS-IPA, mSPECS-IPA-CAIPIRINHA and mSPECS-IPA-CAIPIVAT for slice 3.

Similar to the simulation reconstructed results section, we also investigated the *SNR* value and the activation detection rate from the reconstructed brain images of the experimental fMRI data. Figure 12 shows the *SNR* and the activation detection rate for ROI of slice 3 from the mSPECS-IPA, mSPECS-IPA-CAIPIRINHA, and the mSPECS-IPA-CAIPIVAT method of the experimental fMRI data. As Figure 12 shows the mSPECS-IPA-CAIPIVAT has the highest average *SNR* value for ROI and the mSPECS-IPA-CAIPIRINHA has the lowest average *SNR* value for ROI. Moreover,

comparing the activation detection rate between these three approaches, the mSPECS-IPA-CAIPIVAT provides the highest average z-score of ROI and the mSPECS-IPA-CAIPIRINHA provides the lowest average z-score of ROI. Compared with the mSPECS-IPA and mSPECS-IPA-CAIPIRINHA approaches, the mSPECS-IPA-CAIPIVAT has a more complete and detailed anatomical structure. Therefore, similar to the conclusion from simulation reconstruction results, the mSPECS-IPA-CAIPIVAT method has a higher accuracy capturing the task-related activation signal compared with the non-image shift techniques.

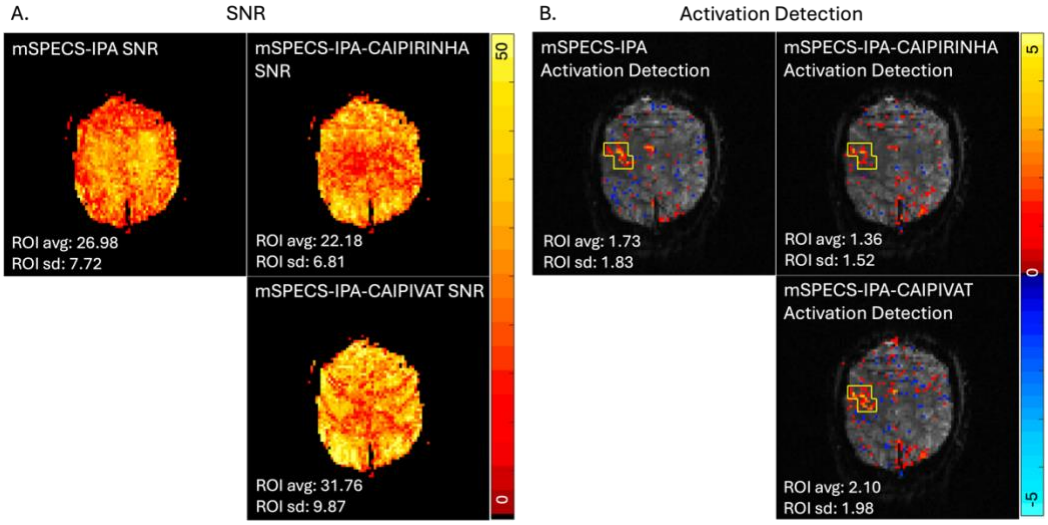

Figure 12. The average *SNR* and the average activation detection rate of ROI for slice 3 from mSPECS-IPA, mSPECS-IPA-CAIPIRINHA and mSPECS-IPA-CAIPIVAT model of the experimental fMRI data.

5. Experimental FMRI Study

In this study, we introduce a novel SMS technique called the mSPECS-IPA-CAIPIVAT model, which incorporates unique imaging shift methods. We also incorporate a novel two-dimensional Hadamard phase encoding technique to increase the size of the aliasing matrix. Bootstrapping and artificial aliasing of calibration images are also included in our model. We applied our model to the simulated fMRI data and the in vivo experimental fMRI data and compared the reconstructed results with previous models, mSPECS-IPA. We can conclude that compared with the previous model, our model can reduce the scan time by incorporating the subsampling method, but at the same time, still can generate high-quality and high-resolution reconstructed images. Also, our model can capture more activation information from the functional dataset.

Acknowledgments

The authors thank the Wehr Foundation as this research is funded by the Computational Sciences Summer Research Fellowship (CSSRF) at Marquette University in the Department of Mathematical and Statistical Sciences.

Reference

Barth, M., Breuer, F., Koopmans, P. J., Norris, D. G. and Poser, B. A. *Simultaneous multislice (SMS) imaging techniques*. Magn Reson Med, 2016. 75(1):63--81.

Breuer, F. A., Blaimer, M., Heidemann, R. M., Mueller, M. F., Griswold, M. A. and Jakob, P. M. *Controlled aliasing in parallel imaging results in higher acceleration (CAIPIRINHA) for multi-slice imaging.* Magn Reson Med, 2005. 53(3):684--91.

Cho, Z. H., Kim, D. J., and Kim, Y. K. *Total inhomogeneity correction including chemical shifts and susceptibility by view angle tilting*. Medical physics, 1988. 15(1), 7-11.

Griswold, M. A., Jamob, P. M., Heidemann, R. M., Nikkka, M., Jellus, V., Wang, J., Kiefer, B. and Haase, A. *Generalized autocalibrating partially parallel acquisition (GRAPPA)*. Magn Reson Med, 2002. 47:1202–1210.

Hyde, J. S., Jesmanowicz, A., Froncisz, W., Kneeland, J. B., Grist, T. M. and Campagna, N. F. *Parallel image acquisition from noninteracting local coils*. Journal of Magnetic Resonance, 1986. 70(3), 512-517.

Jungmann, P. M., Ganter, C., Schaeffeler, C. J., Bauer, J. S., Baum, T., Meier, R. and Woertler, K. *View-Angle Tilting and Slice-Encoding Metal Artifact Correction for Artifact Reduction in MRI: Experimental Sequence Optimization for Orthopaedic Tumor Endoprostheses and Clinical Application*. PLoS One, 2015. 10(4):e0124922.

Kociuba, C. M. *A Fourier description of covariance, and separation of simultaneously encoded slices with in-plane acceleration in fMRI*. Ph.D. Dissertation, 2016. Marquette University, Milwaukee, Wisconsin, USA.

Mansfield P. *Multi-planar image formation using NMR spin echoes*. Journal of Physics C: Solid State Physics, 1977. 10(3): L55.

Min-Oh Kim, Sang-Young Zho and Dong-Hyun Kim. *3D imaging using magnetic resonanace tomosynthesis (MRT) technique*. Med. Phys, 2012. 39(8): 4733-4741.

Min-Oh Kim, Taehwa Hong and Dong-Hyun Kim. *Multislice CAIPIRINHA Using View Angle Tilting Technique (CAIPIVAT).* Tomography, 2016. 43-48.

Ogawa, S., Lee, T. M., Kay, A. R. and Tank, D. W. *Brain magnetic resonance imaging with contrast dependent on blood oxygenation*. Proc Natl Acad Sci USA, 1990 Dec. 87(24):9868-721.

Pruessmann, K. P., Weiger, M., Scheidegger, M. B. and Boesiger, P. *SENSE: Sensitivity Encoding for Fast MRI*. Magn Reson Med, 1999. 42:952–962.

Rowe, D. B., Bruce, I. P., Nencka, A. S., Hyde, J. S. and Kociuba, M. C. *Separation of parallel encoded complex-valued slices (SPECS) from a signal complex-valued aliased coil image*. Magn Reson Imaging, 2016. 34(3):359-69.

Rowe, D. B. and Logan, B. R. *A complex way to compute fMRI activation*. Neuroimage, 2004. 23(3):1078-92.

Rowe, D. B., Nencka, A. S., Jesmanowicz, A. and Hyde, J. S. *Separation of two simultaneously encoded slices with a single coil*. In Proc Intl Soc Magn Reson Med, 2013. Vol. 21, p. 0123.

Rzedzian, R., Mansfield, P., Doyle, M., Guilfoyle, D., Chapman, B., Coupland, R. E., Chrispin, A. and Small, P. *Real-time nuclear magnetic resonance clinical imaging in pediatrics*. The Lancet, 1983. 322:1281-2.

Sakitis, C. J., Brown, D. A., Rowe, D. B. *A Bayesian complex-valued latent variable model applied to functional magnetic resonance imaging*. J Royal Stat Soc, Series C 2024. https://doi.org/10.1093/jrsssc/qlae046.

Setsompop, K., Gagoski, B. A., Polimeni, J. R., Witzel, T., Wedeen, V. J. and Wald, L. L. *Blipped-controlled aliasing in parallel imaging (blipped-CAIPI) for simultaneous multi-slice EPI with reduced g-factor penalty*. Magn Reson Med, 2012. 67(5): 1210-1224.

Souza, S. P., Szumowskim, J., Dumoulin, C. L., Plewes, D. P. and Glover, G. *SIMA - simultaneous multislice acquisition of MR images by Hadamard-encoded excitation*. J Comput Assist Tomogr, 1988. 12:1026–1030.

Stehling, M. K., Turner, R., and Mansfield, P. *Echo-planar imaging: magnetic resonance imaging in a fraction of a second*. Science, 1991. *254*(5028), 43-50.

Welvaert, M. and Rosseel, Y. *On the Definition of Signal-To-Noise Ratio and Contrast-To-Noise Ratio for fMRI Data*. J PloS ONE, 2013. 8(11): e77089.